Logic-based machine learning predicts how escitalopram attenuates cardiomyocyte hypertrophy

Taylor G. Eggertsen, Joshua G. Travers, Elizabeth J. Hardy, Matthew J. Wolf, Timothy A. McKinsey, and Jeffrey J. Saucerman

Contact: jsaucerman@virginia.edu

ABSTRACT

Introduction

Cardiomyocyte hypertrophy is a key clinical predictor of heart failure. High-throughput and AI-driven screens have potential to identify drugs and downstream pathways that modulate cardiomyocyte hypertrophy.

Methods

Here we developed LogiRx, a logic-based mechanistic machine learning method that predicts drug-induced pathways. We applied LogiRx to discover how drugs discovered in a previous compound screen attenuate cardiomyocyte hypertrophy. We experimentally validated LogiRx predictions in neonatal cardiomyocytes, adult mice, and two patient databases.

Results

Using LogiRx, we predicted anti-hypertrophic pathways for 7 drugs currently used to treat non-cardiac disease. We experimentally validated that escitalopram (Lexapro) and mifepristone inhibit hypertrophy of cultured cardiomyocytes in two contexts. The LogiRx model predicted that escitalopram prevents hypertrophy through an "off-target" serotonin receptor/PI3Kγ pathway, mechanistically validated using additional investigational drugs. Further, escitalopram reduced cardiomyocyte hypertrophy in a mouse model of hypertrophy and fibrosis. Finally, mining of both FDA and University of Virginia databases showed that patients with depression on escitalopram have a lower incidence of cardiac hypertrophy than those prescribed other serotonin reuptake inhibitors that do not target the serotonin receptor.

Conclusion

Mechanistic machine learning by LogiRx discovers drug pathways that perturb cell states, which may enable repurposing of escitalopram and other drugs to limit cardiac remodeling through "off-target" pathways.

30 **INTRODUCTION**

31 Cardiac hypertrophy is a key clinical predictor of heart failure[1–5]. Hypertrophy is a response to
32 various physiological stressors, such as pressure overload, drug toxicity, or gene mutations[6]. Several
33 drugs prescribed for heart failure also affect cardiac hypertrophy, such as angiotensin converting
34 enzyme (ACE) inhibitors, beta blockers, and angiotensin receptor blockers (ARBs)[7]. But heart failure
35 rates are still rising, with a five year mortality rate > 40%[8]. There has been increasing effort towards drug
36 repurposing for cardiovascular indications to accelerate translation and reduce cost[9,10]. One such
37 success is the repurposing of SGLT2 inhibitors from diabetes to cardiovascular disease[11].

38 Numerous medications not initially designed for cardiac treatment impact the progression of
39 cardiac hypertrophy[12–15], although their mechanisms are largely unknown. Experimental approaches to
40 prioritize drugs from large screens and investigate their mechanisms are time intensive and costly. Drug
41 development is further hindered by the complexity of hypertrophic signaling, with a high degree of
42 cross-talk between multiple molecular pathways[7,16]. Protein interaction databases and gene regulatory
43 networks have been used previously to explore drug target interactions[17,18], however these studies have
44 primarily examined network topology rather than simulating network response to drugs.

45 To address the challenges of mapping and mechanistically understanding drug responses from
46 phenotypic screens, we developed a logic-based predictor of drug pathways (LogiRx). LogiRx maps from
47 drug-target and protein interaction databases to curated logic-based network models of cell phenotype.
48 We used LogiRx to prioritize seven anti-hypertrophic drugs identified in a previous cell-based screen[12],
49 providing mechanistic insight to how two drugs attenuate hypertrophy via “off-target” pathways. LogiRx
50 predictions were experimentally validated in cultured cardiomyocytes, mice, and in two patient
51 databases of electronic health records. Together, these studies validate the LogiRx method and provide
52 mechanistic insights into how escitalopram (Lexapro) and other drugs modulate cardiomyocyte
53 hypertrophy.

54

55 **METHODS**

56 **Linking drug targets to logic-based signaling network using LogiRx**

57 We used a published logic-based differential equation model of the cardiomyocyte hypertrophy
58 signaling network[19]. This literature-based network of proteins and genes is composed of 107 nodes
59 (proteins or mRNAs) and 193 edges, validated against 450 experiments across the literature with 77%
60 accuracy[20]. The model correctly predicted the anti-hypertrophic effect of 28 out of 32 drug responses
61 from our previous experimental screen[12].

62 **Linking drug targets to logic-based signaling network using LogiRx**

63 We first identified hits from a previous screen for compounds that inhibit cardiomyocyte
64 hypertrophy[12], identifying protein targets using the drug-target database DrugBank[21] (**Figure 1A**). LogiRx
65 identified top scoring directed pathways from drug targets to the hypertrophy signaling network nodes
66 through Omnipath directed interactions[22,23] using the PathLinker algorithm[24,25] in Cytoscape[26] (**Figure**
67 **1B**). Top scoring candidate drug pathways were added to a LogiRx-expanded logic-based network model
68 using Netflux.

69 **Literature validation of LogiRx-expanded models**

70 The LogiRx-expanded logic-based differential equation model was simulated to test the
71 functional impact of the drug pathways on cardiomyocyte hypertrophy. Each pathway was individually
72 added to the signaling network model to create expanded logic-based differential equation model
73 variants. Each drug-pathway-expanded model was simulated to predict the semi-quantitative network
74 dynamics in response to drug. To assess the functional validity of the LogiRx-identified drug pathways,
75 we validated their performance against 450 literature experiments previously used to validate the
76 hypertrophy signaling model[20] (**Figure 1C**).

77 **Simulating drug mechanisms of action**

78 Drug mechanisms of action were implemented using logic-based equations as described
79 previously[27,28], accounting for mechanisms of drug action (agonist or antagonist) and drug binding
80 (competitive or non-competitive). The binding properties determine how the upstream signal is shifted
81 by the drug dose, while the drug action determines whether the target node is upregulated (agonist) or
82 downregulated (antagonist). Each simulation was run first without drug input to establish baseline
83 activity, and then with the appropriate drug to identify steady-state changes in drug response.

84 **Mechanistic subnetwork analysis**

85 To identify pathways mediating drug response, we utilized the mechanistic subnetwork
86 method[27–29]. We simulated the global response of the network to the drug in the presence of
87 hypertrophic stimulus to identify "drug-responsive nodes". We then simulated knockdown of each node
88 and measured that node's influence on drug-induced change in cardiomyocyte hypertrophy, referring to
89 these nodes as "regulating nodes". The intersection of the regulating nodes with responsive nodes
90 results in a mechanistic subnetwork that maps the pathways mediating drug activity. Thus, LogiRx
91 combines drug-target and protein interaction databases, path optimization, and logic-based network
92 simulations to obtain mechanistic subnetworks that explain drug response.

93 **Experimental validation in cardiomyocytes**

94 We isolated neonatal cardiomyocytes using the NeoMyts kit from Cellutron as described
95 previously[28]. Cardiomyocytes were cultured with serum for 24 hr in 96-well microplates, followed by a
96 24 hr serum starve. Cardiomyocytes were then treated with one of two hypertrophic stimuli (10 μM
97 phenylephrine, 5 ng/ml transforming growth factor β), 10% FBS (positive control), or serum-free media
98 alone (negative control). At the same time, cells were treated with specified concentrations of the
99 appropriate compound (escitalopram, mifepristone, paroxetine, sarpogrelate hydrochloride, or
100 AL082D06) for 48 hrs.

101 To prepare for immunofluorescent imaging, cardiomyocytes were first fixed with 4%
102 paraformaldehyde for 20 min, and then permeabilized with 0.1% Triton-X for 15 min. Cardiomyocytes
103 were blocked with 1% bovine serum albumin in PBS for 1 hr, then treated with mouse anti-α-actinin
104 primary antibody (Sigma-Aldrich Cat#A7811, RRID:AB_476766) at a concentration of 1:200 overnight.
105 Cardiomyocytes were blocked with 5% goat serum in PBS for 1 hr, then Alexa Fluor-568-conjugated goat
106 anti-mouse secondary antibody (Thermo Fisher Scientific Cat#A11031, RRID:AB_144696) at a
107 concentration of 1:200 was applied for 1 hr. The cells were stained with DAPI prior to imaging.
108 High-content imaging was performed on the stained cardiomyocytes using an Operetta CLS High
109 Content Analysis System. These images were processed using CellProfiler[30] using a cellular segmentation
110 algorithm developed previously and validated to within 5% of two independent manual
111 segmentations[31]. Median cell area was used as a representative measure of the cell population in each
112 well, and cells with undetectable cytoplasm were not counted.
113 Total protein was isolated from neonatal rat ventricular myocytes (NRVM) using RIPA lysis buffer
114 (25 mM Tris pH 7.6, 150 mM NaCl, 1% NP-40, 1% sodium deoxycholate and 0.1% SDS) supplemented
115 with Halt™ protease and phosphatase inhibitor cocktail (ThermoFisher 78442). Proteins were separated
116 using SDS-PAGE and transferred onto nitrocellulose membrane (0.45 μm, Thermo Scientific 88018).
117 Total protein was first evaluated using LI-COR Revert™ 520 Total Protein Stain (926-10021), followed by
118 blotting with antibodies directed against phosphorylated protein kinase D (1:1,000; CST 2051) and
119 glyceraldehyde phosphate dehydrogenase (1:5,000; Proteintech 60004-1-Ig) overnight at 4°C in
120 intercept® (TBS) Blocking Buffer (LI-COR 927-60001) containing 0.2% Tween-20. Following incubation
121 with primary antibodies, blots were rinsed and probed with appropriate IRDye® secondary antibodies
122 (LI-COR). Protein bands were visualized using a LI-COR Odyssey XF scanner.
123 **Angiotensin II / Phenylephrine Infusion in Mice**

124 All animal procedures were performed in accordance with the Institutional Animal Care and Use
125 Committee at the University of Colorado Anschutz Medical Campus. Ten-week-old male C57BL/6J were
126 purchased from The Jackson Laboratory (Strain # 000664). Alzet mini-osmotic pumps (Model 2004), or
127 mock pumps for Sham animals, were implanted in a subcutaneous pocket created at the suprascapular
128 region under isoflurane anesthesia. Osmotic pumps were prepared to deliver 1.5 μg/kg/day Angiotensin
129 II (Bachem H-1705.0100) and 50 μg/g/day (R)-(-)-Phenylephrine hydrochloride (Sigma P6126) to induce
130 systemic hypertension, cardiac hypertrophy and fibrosis. Beginning 24 hours post-osmotic pump
131 implantation, animals were randomly divided into groups receiving 10 mg/kg/day escitalopram oxalate
132 (Selleckchem S4064) in 10% DMSO dissolved in 10% (2-hydroxypropyl) β-cyclodextrin (Sigma H107) in
133 water, or vehicle control, for 14 days.

134 **Echocardiographic Assessment of Cardiac Structure and Function**

135 Serial transthoracic echocardiographic and Doppler analysis were performed using the
136 VisualSonics Vevo F2 instrument. Animals were anesthetized with 2% isoflurane, hair on the chest was
137 removed using a chemical depilatory, and body temperature maintained at 37°C. Isoflurane was
138 maintained at 1.5% throughout the procedure to ensure a consistent plane of anesthesia across
139 subjects. Parasternal long axis (PSLAX) and parasternal short axis (SAX) views of the left ventricle were
140 obtained; SAX two-dimensional views of the LV at the level of the papillary muscle were used to acquire
141 M-mode images. Anterior and posterior LV wall thickness and internal diameters were measured in
142 systole and diastole using these M-mode images. Mitral inflow Doppler signals and myocardial tissue
143 movement of the mitral annulus were obtained to calculate the ratio of early and active filling waves of
144 blood flow through the mitral valve and ventricular tissue velocity to assess cardiac diastolic function.
145 Speckle-tracking strain analyses were acquired from PSLAX B-mode videos. All echocardiographic
146 measurements and analyses were averaged from at least four cardiac cycles and analyses were
147 performed in a blinded manner by a dedicated small animal echocardiography team.

148 **Tissue Procurement**

149 At study endpoint, animals were sacrificed by exsanguination and hearts excised and placed in
150 ice-cold saline. Right ventricular (RV) tissue was dissected from the LV by cutting along the septum and
151 the outer wall of the LV, and all parts weighed. 50 mg base and apical biopsies of the LV were flash-
152 frozen in liquid nitrogen for subsequent biochemical analysis. A cross-section of the LV at the level of the
153 papillary muscles was fixed in 4% PFA in PBS overnight at 4°C followed by preservation in a 30% sucrose
154 solution and embedding in OCT.

155 **Histological Analyses**

156 Frozen tissue sections were cut at a thickness of 10 μm. To evaluate total ventricular fibrotic
157 area, cardiac sections were stained with Picrosirius red dye (0.1% Direct Red 80 in saturated picric acid
158 solution) for 1 hour at room temperature. Whole-heart images were acquired using the image stitching
159 feature on a Keyence BZ-X710 All-in-One Fluorescence Microscope. Fibrotic area was determined by
160 quantifying the ratio of positively stained (red) pixels to the total pixel number of each section (reported
161 as percent collagen content) using ImageJ. In addition, individual cardiomyocyte hypertrophy was
162 assessed by staining cardiac sections with Alexa Fluor 647 wheat germ agglutinin (ThermoFisher
163 W32466) according to manufacturer instructions. Briefly, sections were incubated in a 5.0 μg/mL WGA
164 conjugate solution in HBSS for 10 minutes at room temperature, followed by mounting in ProLong™
165 Glass Antifade Mountant (ThermoFisher P36980). Images were acquired at 40x magnification with the
166 left ventricular free wall using the Keyence BZ-X710 microscope, and individual cardiomyocyte area was
167 quantified using ImageJ.

168 **Patient outcomes associated with drug treatments**

169 To examine whether drugs were correlated with a reduction in cardiac adverse events
170 associated with hypertrophy, we analyzed data from two separate clinical databases. As the first patient
171 cohort, data was collected on November 30th, 2023 from the FDA's Adverse Event Reporting System

172 using the AERSMine tool[32]. The Adverse Event Reporting System is a multi-cohort database containing
173 20 million reports of adverse events from healthcare providers and consumers across the United States.
174 As a second patient cohort, on January 2nd, 2024 we collected data from the University of Virginia Health
175 System Network using the TriNetX tool, which provided access to electronic medical records from
176 approximately 1.7 million patients.

177 This retrospective study is exempt from informed consent. The data reviewed is a secondary
178 analysis of existing data, does not involve intervention or interaction with human subjects, and is de-
179 identified per the de-identification standard defined in Section §164.514(a) of the HIPAA Privacy Rule.
180 The process by which the data is de-identified is attested to through a formal determination by a
181 qualified expert as defined in Section §164.514(b)(1) of the HIPAA Privacy Rule. This formal
182 determination by a qualified expert refreshed on December 2020.

183 **Statistics**

184 All data are presented as the mean ± SEM. Analysis of experimental conditions considered two
185 distinct cardiomyocyte isolations and multiple conditions, with multiple wells in each experiment. For
186 this reason, a two-way ANOVA followed by Dunnett's test for multiple comparisons was selected for
187 statistical calculation. In vivo data were analyzed by ordinary one-way ANOVA followed by Tukey's
188 multiple comparisons test. GraphPad Prism 9 was used for statistical analysis. For all analyses, a p-value
189 <0.05 was considered statistically significant.

190

191 **RESULTS**

192 **Identified drug pathways driving cardiomyocyte hypertrophy**

193 Previously, we performed a microscopy-based screen for drugs that decreased hypertrophy of
194 cardiomyocytes in the presence of phenylephrine[12]. In that study, 94 of 3241 small molecule compounds
195 decreased both cell area and ANP protein expression by at least 70% and did not exhibit cardiotoxicity.

196 In a previous study, we identified that the hypertrophy signaling model was directly targeted by 32 of
197 these 94 drugs, and that the model could mechanistically predict reduction in hypertrophy with 88% (28
198 of 32) prediction accuracy [28]. The remaining 62 of 94 compounds do not target this previous
199 hypertrophy model and presumably inhibit cardiomyocyte hypertrophy through less-characterized
200 mechanisms. Therefore, in this study we sought to identify novel pathways linking the remaining 62
201 compounds to hypertrophy. To identify new drug pathways, we developed a logic-based network
202 predictor of drug pathways (LogiRx) that identifies and simulates molecular pathways that mediate how
203 drugs regulate cell phenotype.

204 As a first application, we employed LogiRx to identify proteins that are directly targeted by the
205 62 anti-hypertrophic compounds from our prior screen[12]. LogiRx analysis mapped 28 of the 62
206 compounds to 79 protein targets in the OmniPath protein interaction database (**Figure 1A**). 11 of 28
207 compounds were successfully mapped to the hypertrophy network via 214 candidate drug pathways
208 (**Figure 1B**). These pathways link 11 drugs and their drug targets to 89 proteins in the network, covering
209 42% of the network. Most of the candidate drug pathways (76%) connect the drug target to the
210 network via an intermediate protein that is not in the original network model, demonstrating the value
211 of pathway inference. Together, the 214 candidate drug-target-network pathways predict mechanisms
212 that may help explain the experimentally-demonstrated anti-hypertrophic effect of these 11
213 compounds.

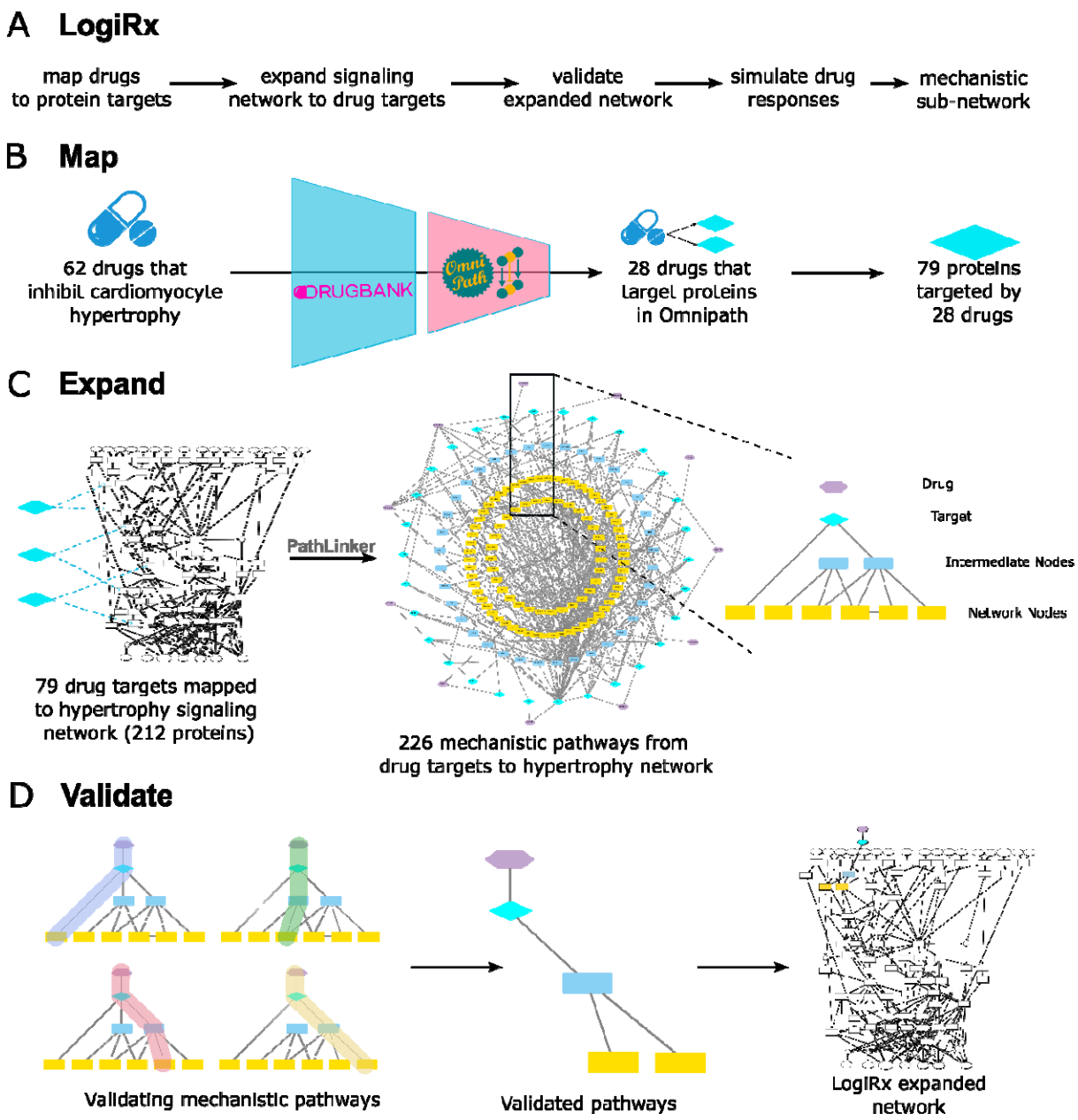

Figure 1. LogiRx discovers pathways from anti-hypertrophic drugs to the cardiomyocyte hypertrophy signaling network. A) Overview of the LogiRx workflow, from drugs to mechanistic predictions. B) Drug targets are identified from DrugBank and filtered by annotations in the protein-interaction database Omnipath. C) Drugs and their protein targets are mapped to the hypertrophy network through LogiRx. D) Drug pathways are individually simulated using Netflux and validated against prior experimental

220 literature. Drug pathways that maintain model validation accuracy are used to expand the hypertrophy
221 network for drug predictions.
222
223 **Logic-based network expansion to predict how drugs regulate hypertrophy**
224 To predict the impact of these drug pathways on cardiomyocyte hypertrophy, logic-based
225 differential equation model variants were created from LogiRx that each simulate the effect of
226 incorporating individual pathway (**Figure 1C**). Each model variant was tested by simulating inhibition of
227 the drug target in the presence of hypertrophic agonist phenylephrine. Most drug pathways were
228 predicted to strongly inhibit hypertrophy (**Figure 2A**). However, some drug pathways reduced the model
229 accuracy when tested against a previous set of 450 experiments, indicating that they are not fully
230 compatible with the mechanisms established in the validated network model (**Figure 2A**).
231 Drug pathways corresponding to 8 of the 11 drugs were predicted to inhibit phenylephrine-
232 induced hypertrophy while maintaining model accuracy above 78%. New LogiRx-expanded drug models
233 were developed combining all relevant validated pathways for each of the 8 drugs. The hypertrophic
234 effect of each drug was simulated using a pharmacological inhibition model based on known drug-target
235 binding mechanisms[27]. Seven of these eight drugs were predicted to be anti-hypertrophic, with context-
236 dependent efficacy depending on the hypertrophic stimulus (**Figure 2B**). 7 of 8 drugs regulated
237 hypertrophy via multiple protein targets.
238

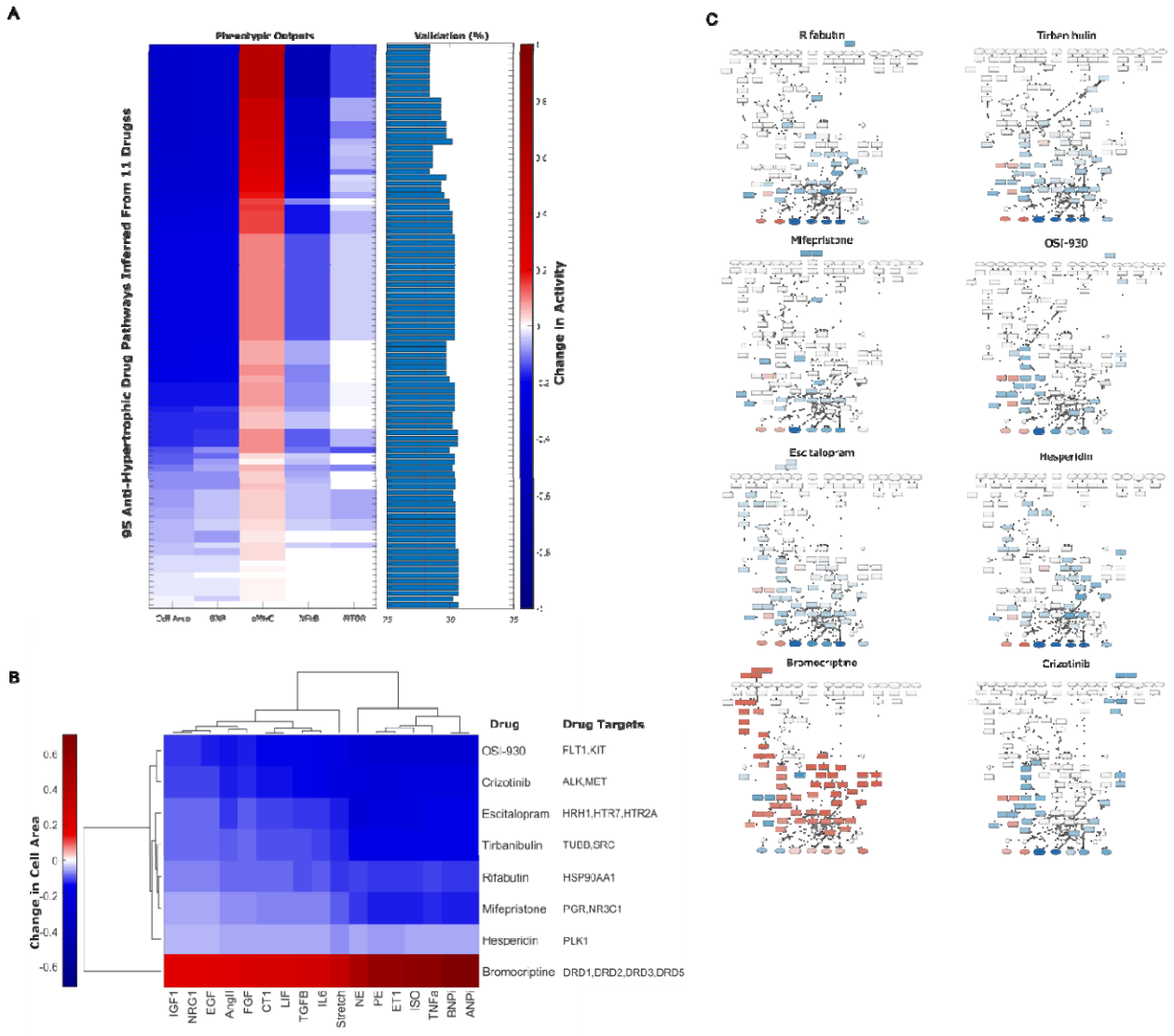

Figure 2. LogiRx-based network model expansion predicts pathways by which drugs affect cardiomyocyte hypertrophy. A) Hypertrophy network variants expanded by individual drug pathways were simulated for their effect on five hypertrophic outputs, as well as validated against 450 experiments from prior literature. Drug pathway annotation is provided in **Supplementary Figure S1**. B) 8 drugs were predicted to affect cardiomyocyte hypertrophy with varying efficacy across 17 biochemical environments. C) Drugs were predicted to inhibit hypertrophy via distinct regional modulation of the hypertrophy signaling network, indicating distinct inhibitory mechanisms.

248 Seven drugs were predicted by the LogiRx-expanded network model to inhibit hypertrophy –
249 OSI-930, crizotinib, escitalopram, tirbanibulin, rifabutin, mifepristone, and hesperidin, representing a
250 variety of drug targets and clinical applications. OSI-930 is an FLT1 and KIT inhibitor that is designed to
251 target cancer cell proliferation in solid tumors[33]. Crizotinib, an ALK and MET inhibitor, is used to treat
252 non-small cell lung cancer but has known cardiac toxicity[34,35]. Escitalopram targets SERT and is used to
253 treat depression and anxiety[36,37]. Tirbanibulin targets TUBB and SRC to treat actinic keratosis, and is
254 being investigated as a potential treatment for acute myeloid leukemia[38]. Rifabutin inhibits HSP90AA1
255 and is an antibiotic preventing mycobacterium avium complex in HIV patients[39]. Mifepristone, which
256 targets both PGR and NR3C1, is commonly used as an abortifacient, but is additionally used to treat
257 diabetic patients with Cushing's syndrome[40]. Hesperidin is a flavonoid and natural supplement currently
258 investigated for anti-inflammatory benefits[41]. Similar to their target diversity, these 8 drugs were
259 predicted to inhibit cardiomyocyte hypertrophy through distinct areas of the hypertrophy network
260 (**Figure 2C**).
261
262 **Experiments in cardiomyocytes validate that escitalopram and mifepristone inhibit hypertrophy**
263 We further prioritized escitalopram, tirbanibulin, mifepristone, OSI-930, and rifabutin for
264 experimental validation based on their relative cardiac safety[33,42–47] and approval status. Neonatal rat
265 cardiomyocytes were treated with PE along with each of these five drugs for 48 h. Consistent with the
266 LogiRx model predictions, tirbanibulin, escitalopram, and mifepristone inhibited PE-induced
267 cardiomyocyte hypertrophy (**Figure 3A-B**). In contrast, OSI-930 and rifabutin did not inhibit hypertrophy
268 even at increased concentrations.
269 While the network analysis in **Figure 2C** predicted that escitalopram would work via
270 downstream hypertrophic pathways that are relatively context-independent, an alternative hypothesis
271 may suggest that escitalopram inhibits alpha-1 adrenergic receptor (α1AR) directly in response to

272 phenylephrine. We tested this hypothesis by introducing an alternative hypertrophic stimulus TGFβ, as
273 well as directly measuring phosphorylation of protein kinase D (PKD), which is proximal to the α1
274 adrenergic receptor in cardiomyocytes. TGFβ-induced hypertrophy was inhibited by both escitalopram
275 and mifepristone (**Figure 3C-D**). Further, while we observed a robust increase in phospho-PKD levels in
276 cardiomyocytes treated with phenylephrine stimulation, no reduction in PKD phosphorylation was
277 observed in cardiomyocytes co-treated with escitalopram (**Figure 3E**). Together, these data indicate that
278 escitalopram antagonizes hypertrophy through downstream mechanisms distinct from blockade of the
279 α1AR.

280 To identify how mifepristone inhibits cardiomyocyte hypertrophy, we performed mechanistic
281 subnetwork analysis. Although the LogiRx network model included drug pathways for mifepristone via
282 both progesterone receptors and glucocorticoid receptors, LogiRx predicted that mifepristone inhibits
283 cardiomyocyte hypertrophy predominantly via inhibition of the glucocorticoid receptor via LCK/ERK and
284 CEBPβ (**Supplementary Figure S2A-B**). We experimentally validated that the glucocorticoid receptor
285 antagonist AL082D06 phenocopied the effects of mifepristone by preventing hypertrophy with PHE or
286 TGFβ (**Supplementary Figure S2C-D**).

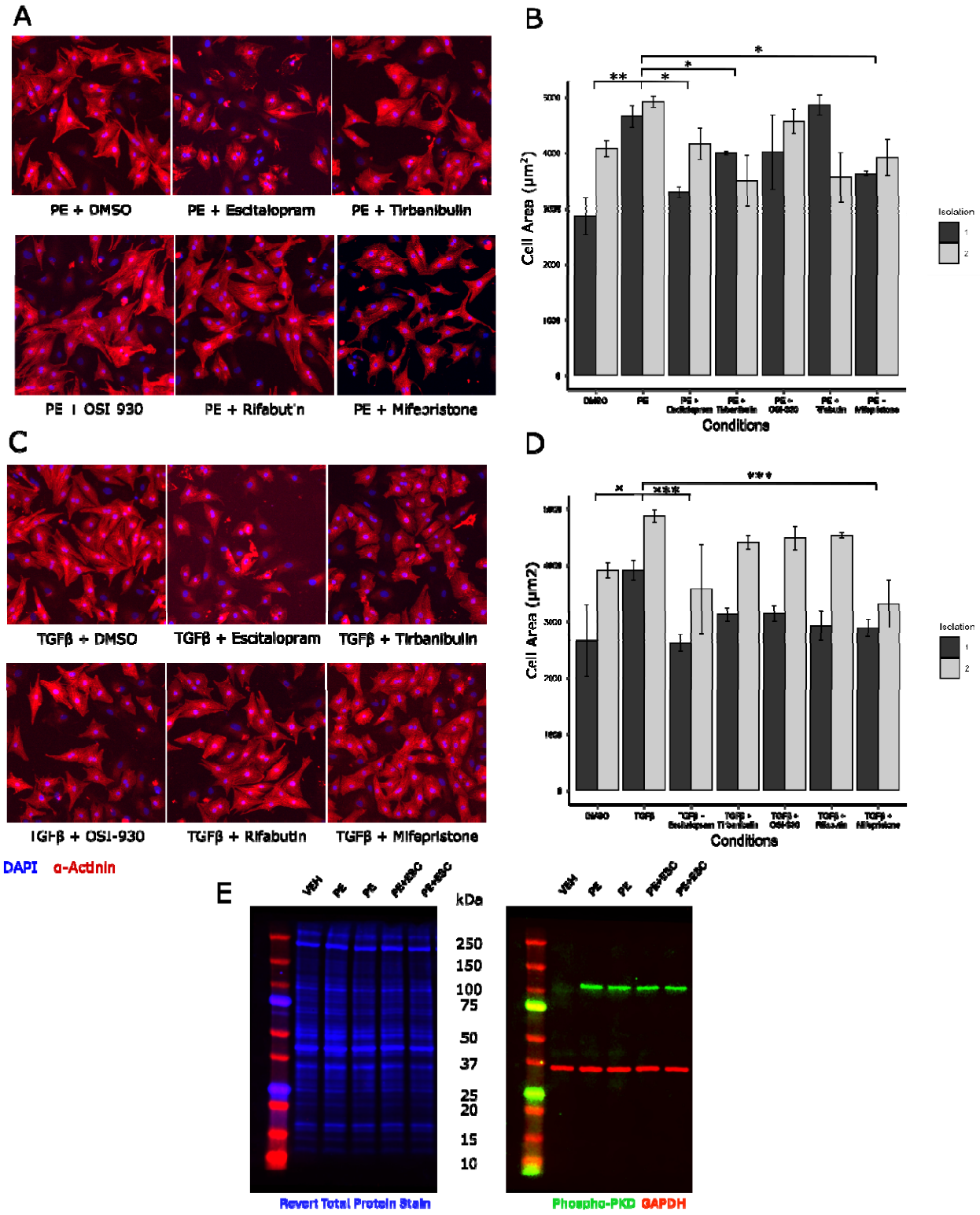

Figure 3. Escitalopram and mifepristone inhibit cardiomyocyte hypertrophy induced by either phenylephrine or TGFβ. The effect of five drugs on PE-induced hypertrophy of neonatal rat

290 cardiomyocytes is shown in A) representative images or B) quantification of automated segmentation.
291 Escitalopram (20 μM), mifepristone (6 μM), and tirbanibulin (6 μM) significantly prevented PE-induced
292 cell area increase over a 48-hour period following treatment. The effect of these five drugs on TGFβ-
293 induced hypertrophy is shown as C) representative images or D) quantification of cardiomyocyte cell
294 area by automated segmentation. Escitalopram (20 μM) and mifepristone (6 μM) significantly prevented
295 TGFβ-induced increase in cell area. E) Western blot of total protein and phospho-PKD in response to PE
296 and/or escitalopram. Two cell isolations were used for each experiment, and a two-way ANOVA was
297 performed followed by a Dunnett's post-hoc test. Error bar indicates SEM, * $p<0.05$, ** $p<0.01$, ***
298 $p<0.001$.
299
300 **Escitalopram inhibits hypertrophy through serotonin receptor and not transporter**
301 As the last stage of LogiRx, we performed mechanistic subnetwork analysis to identify pathways
302 that mediate escitalopram inhibition of cardiomyocyte hypertrophy. We simulated the network-wide
303 response to escitalopram, followed by simulations of network-wide knockdown of each network node in
304 the presence and absence of escitalopram. The intersection of these two analyses resulted in a
305 mechanistic subnetwork that predicted how escitalopram inhibits cardiomyocyte hypertrophy (**Figure**
306 **4A**). This subnetwork predicted that escitalopram inhibits hypertrophy through the serotonin receptor
307 HT2RA, a non-canonical target of escitalopram, rather than as a selective serotonin reuptake inhibitor
308 (SSRI) via the transporter SERT (or SLC6A4). Further, the LogiRx model predicted that the escitalopram-
309 HTR2A pathway acts by inhibiting G-protein signaling to PI3Kγ (**Figure 4A-B**). The model also correctly
310 predicted how αMHC and βMHC gene expression respond to escitalopram (**Supplementary Figure S3**).
311 To experimentally validate these LogiRx predictions, we used sarpogrelate hydrochloride which
312 selectively inhibits HTR2A but not SERT. Prior literature[48,49] demonstrates that sarpogrelate inhibits PE-
313 induced cardiomyocyte hypertrophy both in vitro and in vivo. Our studies confirm that sarpogrelate

314 prevents both PE- and further demonstrates its efficacy against TGFβ-induced cardiomyocyte

315 hypertrophy (**Figure 4C-D**). Downstream of HTR2A, our mechanistic subnetwork predicted Gβγ and PI3K

316 to mediate anti-hypertrophic escitalopram activity. Gβγ directly binds and activates PI3Kγ[50]. To

317 experimentally validate this prediction, we selectively inhibited PI3Kγ with the antitumor drug

318 eganelisib. Eganelisib prevented both PE- and TGFβ-induced cardiomyocyte hypertrophy (**Figure 4E-F**),

319 further validating the non-canonical escitalopram-HTR2A-PI3Kγ pathway predicted by LogiRx.

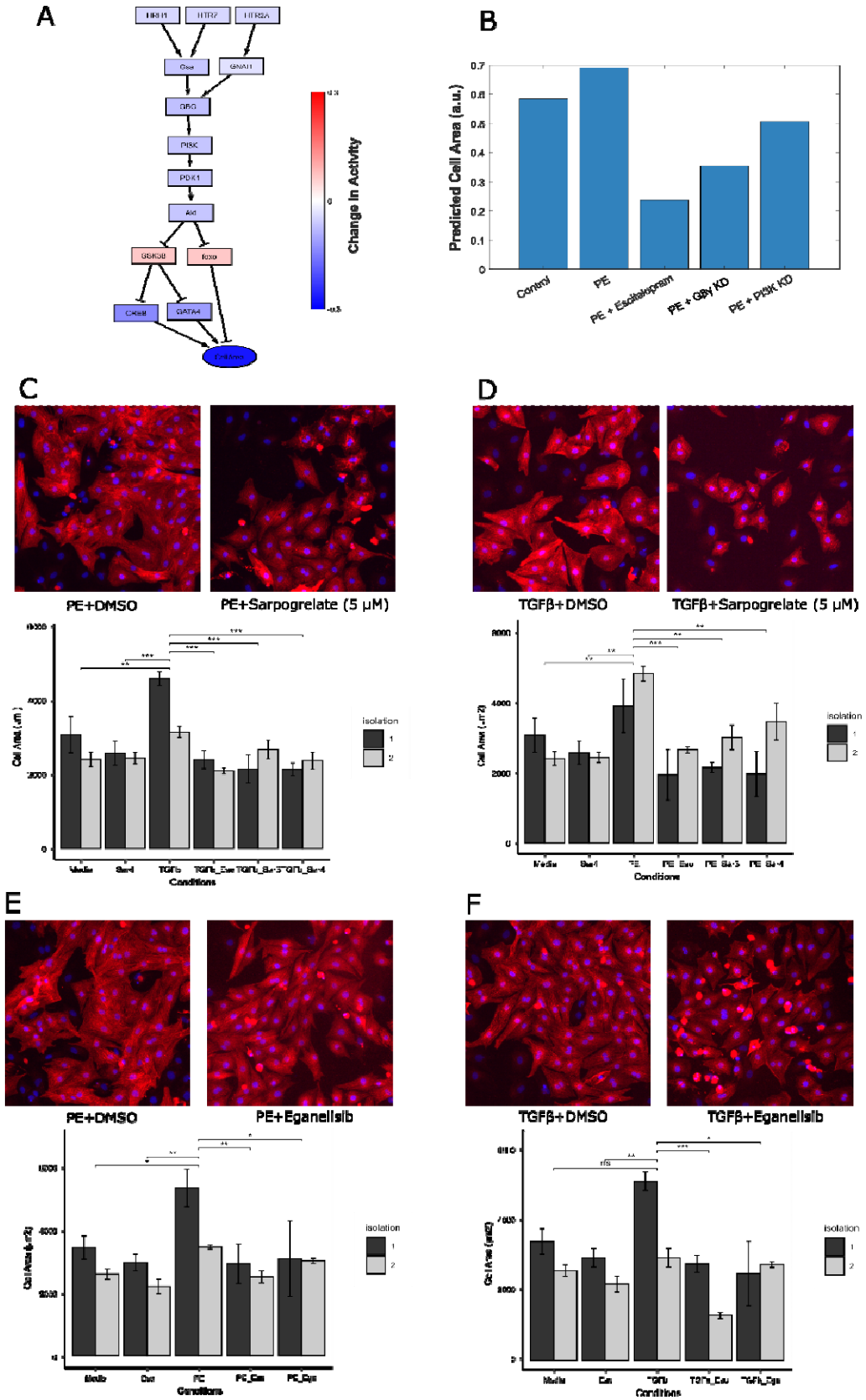
A
B
Predicted Cell Area (a.u.)
Control
PE
PE + Escitalopram
PE + Gβγ KD
PE + PI3K KD
Change In Activity
C
PE+DMSO
PE+Sarpogrelate (5 μM)
D
TGFβ+DMSO
TGFβ+Sarpogrelate (5 μM)
E
PE+DMSO
PE+Eganelisib
F
TGFβ+DMSO
TGFβ+Eganelisib
isolation
Conditions

321 **Figure 4. Escitalopram prevents cardiomyocyte hypertrophy by inhibiting serotonin receptors.** A)
322 Mechanistic subnetwork analysis to predict how escitalopram suppresses cardiomyocyte hypertrophy.
323 B) Simulations of PE-induced hypertrophy and modulation by escitalopram, Gβγ inhibition, or PI3Kγ
324 inhibition. Serotonin receptor inhibitor sarpogrelate hydrochloride (5 µM) significantly prevents C) PE-
325 and D) TGFβ-induced cardiomyocyte hypertrophy 48 hours post treatment, as shown by representative
326 images and quantification of automated segmentation. PI3Kγ inhibitor eganelisib (20 µM) significantly
327 prevents E) PE- and F) TGFβ-induced cardiomyocyte hypertrophy 48 hours post treatment, as shown by
328 representative images and quantification of automated segmentation. Two cell isolations were used for
329 each experiment, and a two-way ANOVA was performed followed by a Dunnett's post-hoc test. Error
330 bar indicates SEM, * $p<0.05$, ** $p<0.01$, *** $p<0.001$.
331
332 **Escitalopram inhibits cardiomyocyte hypertrophy *in vivo***
333 To test whether escitalopram also reduces cardiomyocyte hypertrophy in vivo, escitalopram was
334 delivered to mice subjected to the angiotensin II and phenylephrine (AngII/PE) as a mouse model of
335 cardiac hypertrophy and fibrosis. Angiotensin II (1.5 mg/kg/day) and phenylephrine (50 mg/kg/day)
336 were delivered continuously for 14 days through an osmotic minipump as previously described[51]; daily
337 escitalopram was administered via intraperitoneal injection at 10 mg/kg/day beginning the day after
338 pump implantation (**Figure 5A**). Mice subjected to AngII/PE for 14 days exhibited significant global
339 cardiac hypertrophy, as indicated by heart weight to body weight ratio (HW:BW), as well as a significant
340 increase in LV mass in particular (LV:TL) (**Figure 5B-C**). Furthermore, AngII/PE challenge induced
341 dramatic fibrosis in the LV free wall, which likely also contributed to the increase in overall LV mass
342 (**Figure 5D-E**). Cardiac structure and systolic and diastolic function were evaluated by echocardiography,
343 revealing an increase in LV wall thickness in diastole, which is consistent with the increased HW:BW
344 ratio (**Figure 5F**). Furthermore, AngII/PE mice demonstrated trends towards increases in systolic

345 function, measured by ejection fraction, as well as increases in the E/E' ratio, which is indicative of
346 impaired LV relaxation or diastolic dysfunction (**Figure 5G-H**).
347 Some mice treated with AngII/PE also received daily administration of escitalopram delivered via
348 intraperitoneal injection at 10 mg/kg/day. These animals showed no change in overall collagen content
349 in the LV, suggesting a lack of an effect on the cardiac fibroblast population (**Figure 5D-E**). There was
350 also no significant effect of escitalopram on global cardiac hypertrophy or any functional parameters
351 assessed by echocardiography (**Figure 5B-C,F-H**). However, imaging of cardiomyocyte sections stained
352 with WGA revealed a modest but significant reduction in individual cardiomyocyte hypertrophy in
353 response to treatment with escitalopram (**Figure 5I-J**). In summary, while escitalopram did not offer
354 significant protection against global cardiac hypertrophy or dysfunction in this severe injury model,
355 escitalopram attenuated cardiomyocyte hypertrophy in vivo, consistent with the antihypertrophic effect
356 of escitalopram predicted by LogiRx and measured in cultured cardiomyocytes.
357

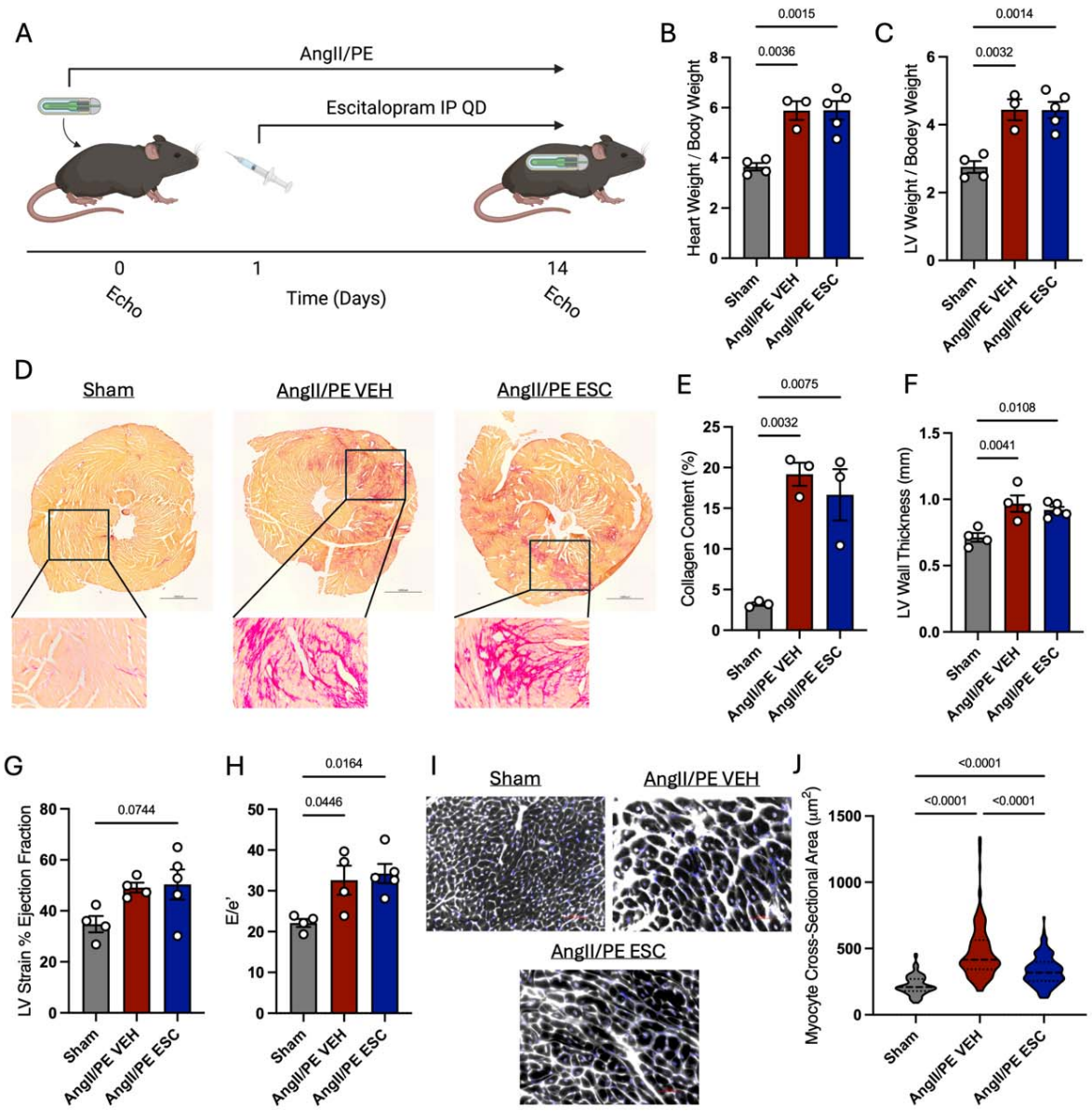

Figure 5. Escitalopram Attenuates Cardiomyocyte Hypertrophy in AngII/PE Mice

A. Schematic of cardiac injury model and escitalopram administration. Mice were continuously delivered AngII/PE through an osmotic minipump to induce cardiac injury and fibrosis, and injected with 10 mg/kg/day escitalopram or vehicle control for 14 days. Quantification of HW:BW (B) and LV:BW (C) ratios. D. Representative picrosirius red staining of heart cross-sectional tissues in sham mice and AngII/PE mice treated with vehicle or escitalopram, and quantification of percent collagen content (E). Results of echocardiographic analyses of AngII/PE mice, showing the left ventricular wall thickness in

365 diastole (F), percent ejection fraction derived from strain analysis (G), and the ratio of early mitral valve
366 flow velocity to mitral annulus velocity by tissue Doppler (E/e') indicating diastolic function. I. Wheat
367 germ agglutinin staining of tissue sections, with quantification of cardiomyocyte cross-sectional area (J).
368 Statistical analyses performed by one-way ANOVA with Tukey's post hoc multiple comparisons test.
369

370 **Cardiac outcomes for patients prescribed escitalopram**

371 Based on consistent anti-hypertrophic roles of escitalopram shown by LogiRx, cultured rat
372 cardiomyocytes, and mouse cardiomyocytes in vivo, we asked whether patients prescribed escitalopram
373 may also exhibit a reduced incidence of cardiac hypertrophy. We first mined patient reports from the
374 FDA Adverse Event Reporting System for incidence of cardiac hypertrophy or failure among patients
375 prescribed escitalopram or related SSRIs that are not known to target HTR2A. Among those diagnosed
376 with depression, patients prescribed escitalopram (which inhibits both SERT and HTR2A) had a lower
377 incidence of left ventricular or ventricular hypertrophy when compared to treatment with other SSRIs
378 sertraline, venlafaxine, and paroxetine that inhibit SERT but not HTR2A (**Figure 6A**). An exception is
379 patients treated with fluoxetine, who had lower incidence of cardiac failure compared to escitalopram
380 treatment.

381 To validate these findings in an independent patient population with more structured data
382 collection, we mined electronic health records from the University of Virginia (UVA) Health System.
383 Among UVA patients diagnosed with depression, those prescribed escitalopram exhibited a statistically
384 lower incidence of left ventricular hypertrophy than those prescribed SSRI paroxetine as well as the
385 serotonin receptor agonist buspirone (**Figure 6B**). To verify the hypertrophy annotation from this
386 analysis, we examined echocardiograms from de-identified patients using the same drug and diagnosis
387 queries. These confirm qualitatively larger interventricular septum thickness (IVSD) and left ventricular
388 posterior wall end diastole (LVPWD) in a patient prescribed paroxetene and diagnosed with hypertrophy

389 than echocardiograms from patients prescribed escitalopram or other SSRIs not diagnosed with

390 hypertrophy (**Figure 6C**). Stratifying patients in the FDA (**Figure 6D**) and UVA (**Figure 6E**) databases by

391 sex, both male and female patients with depression prescribed escitalopram exhibit less hypertrophy

392 than that seen with two or more SSRIs. A reduced rate of hypertrophy was also seen in patients in the

393 FDA database with anxiety on escitalopram compared with other SSRIs (**Supplementary Figure S4**).

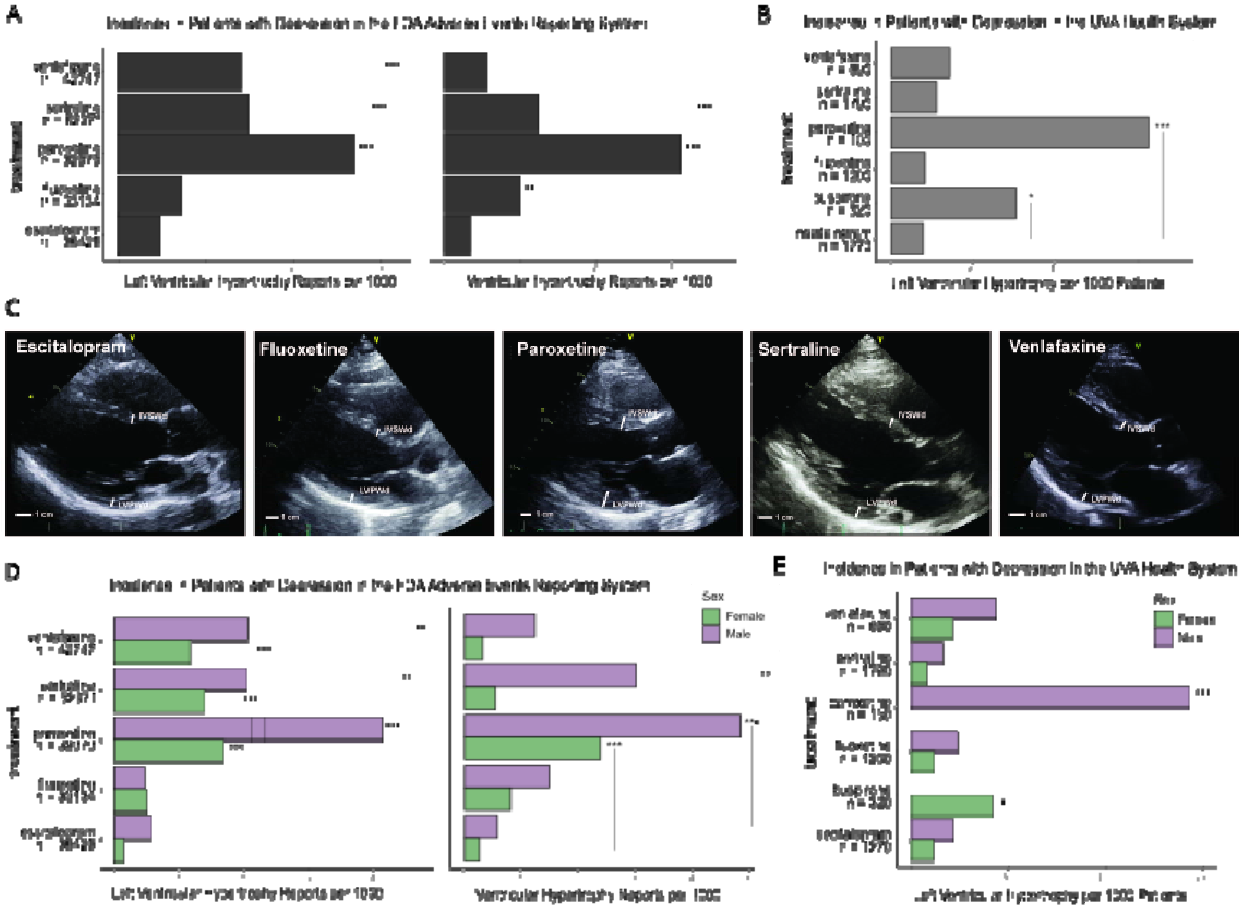

394

395 **Figure 6. In two patient cohorts with depression, those prescribed escitalopram exhibit a lower**

396 **incidence of cardiac hypertrophy than those prescribed other SSRIs.** A) Reports of left ventricular

397 hypertrophy (left) or ventricular hypertrophy (right) per 1000 patients are shown for patients with

398 depression taking either escitalopram or another SSRI (fluoxetine, paroxetine, sertraline, or venlafaxine)

399 in the FDA Adverse Events Reporting System. B) Diagnoses of left ventricular hypertrophy per 1000

400 patients are shown for patients with depression taking either escitalopram or another SSRI in the U.

401 Virginia Health System. C) Verification of echocardiograms from patients in the UVA Health System with
402 hypertrophy (prescribed paroxetine) or without hypertrophy (prescribed escitalopram, fluoxetine,
403 sertraline, or venlafaxine). D) FDA adverse event reports of left ventricular hypertrophy (left) or
404 ventricular hypertrophy (right) per 1000 patients are further divided into incidence by sex. E) Diagnoses
405 of left ventricular hypertrophy in the UVA Health System, divided into incidence by sex. In the UVA
406 Health System, no female patients prescribed paroxetine and no male patients prescribed busipirone
407 exhibited left ventricular hypertrophy. * $p<0.05$, ** $p<0.01$, *** $p<0.001$.
408

409 **Discussion**

410 Despite a strong association between heart failure and hypertrophy, drugs that directly treat
411 hypertrophy are limited[52]. As seen with sildenafil, drug repurposing may provide a rapid translational
412 avenue to identify new therapeutic strategies for cardiac hypertrophy and heart failure[53,54]. Drug
413 repurposing requires sophisticated screening for efficacy but also methods to identify how effective
414 drugs work. In this study we developed a new mechanistic machine learning method, LogiRx, that
415 predicts new pathways that map from drugs to a mechanistic logic-based model of a signaling network.
416 We applied LogiRx to hits from our previous experimental compound screen[12] and predicted the
417 pathways by which 7 of these drugs modulate cardiomyocyte hypertrophy. Experiments in cultured
418 cardiomyocytes validated the context-independent antihypertrophic role of two drugs, escitalopram and
419 mifepristone predicted by LogiRx. Pathways that mediate the effects of escitalopram and mifepristone
420 were predicted by subnetwork analysis, and these predictions were further experimentally validated
421 (escitalopram: serotonin receptors and Gβγ; mifepristone: glucocorticoid receptor). Analysis of
422 electronic health records validate these in silico and in vitro results findings, demonstrating that
423 escitalopram is associated with a lower incidence of cardiac hypertrophy in depression or anxiety

424 patients compared to multiple SSRIs in two large independent populations. Together, these results
425 suggest potential repurposing avenues for escitalopram and mifepristone in cardiac hypertrophy.
426 LogiRx identifies regulatory signaling pathways and dynamic mechanistic predictions that map
427 from drugs to an established signaling network. Several other computational methods construct
428 signaling pathways from both protein-interaction and/or gene expression data[55–57]. Notably, CARNIVAL
429 combines gene expression with protein interaction data to predict upstream signaling pathways that
430 drive changes gene expression changes[58]. LogiRx provides additional benefits of its logic-based
431 differential equation framework that is highly validated for cardiomyocyte hypertrophy[19,20,28,59] to
432 provide dynamic, mechanistic simulations of perturbation experiments (**Figure 2, 4**). The performance of
433 LogiRx depends on the accuracy and completeness of drug, target, and network model resources, as
434 well as the characteristics of the validation experiments. These limitations and potential improvements
435 are described in **Supplementary Table S1**. LogiRx may be most readily applied to settings where
436 annotated drugs have been used to screen cellular phenotype or gene expression, and there is also a
437 validated mechanistic network model that predicts regulation of that cell response. For example, LogiRx
438 may be amenable for integrating drug screens and mechanistic network models in areas such as
439 myofibroblast transformation for fibrosis[60,61] and proliferation for breast cancer[62,63]. Challenges to this
440 approach arise when there is insufficient characterization of drug targets, inadequate relevance of the
441 drug targets to the network model, or an inadequately validated mechanistic network model.
442 Escitalopram (Lexapro) is a commonly prescribed SSRI (>30M prescriptions in the US) with a
443 well-known safety profile[36,37]. Less well understood is the role of SSRIs in cardiac disease. Escitalopram
444 was shown to prevent a diabetic model of cardiac hypertrophy, however the mechanisms remain poorly
445 understood[64]. Our LogiRx model predicts that escitalopram inhibits cardiomyocyte hypertrophy through
446 its off-target HTR2A. This predicted mechanism is supported by our understanding of the role of
447 serotonin receptors HTR2A and HTR2B[65–67] in cardiomyocyte hypertrophy. Escitalopram decreased

448 cardiomyocyte size in cell culture, mice, and was associated with lower incidence of ventricular
449 hypertrophy in patients, but escitalopram did not reduce global heart weight in the mice. We
450 hypothesize that this difference may be due marked fibrosis in this mouse model and partial attenuation
451 of cardiomyocyte hypertrophy by escitalopram (**Figure 5D**).

452 Paroxetine, another SSRI that more specifically targets SERT, was previously shown to prevent
453 left ventricular dysfunction following myocardial infarction through an off-target GRK2 mechanism[68].
454 GRK2 is unlikely to mediate the increased incidence of hypertrophy we found associated with patients
455 prescribed paroxetine, because the clinical concentration is below the IC50 for GRK2[69,70]. Escitalopram
456 off-target of HT2A and paroxetine off-target of GRK2 indicates that other SSRIs may have off-targets that
457 contribute to the differential association with cardiac hypertrophy and failure we observed in patients
458 with depression or anxiety. Further, paroxetine derivatives with enhanced affinity for GRK2 demonstrate
459 the potential for selective repurposing towards "off targets"[71,72].

460 While mifepristone is best known as a progesterone inhibitor, it was originally discovered in a
461 search for glucocorticoid receptor antagonists and is used in Cushing's syndrome with hyperglycemia[40].
462 Glucocorticoids and their receptors have a complex role in cardiovascular health. Glucocorticoid
463 stimulation induces hypertrophy in primary rat cardiomyocytes[73,74], yet mice with cardiomyocyte-
464 specific deletion of glucocorticoid receptor have increased cardiac hypertrophy[75] and direct
465 glucocorticoid receptor inhibition can enhance cardiomyocyte proliferation[76]. LogiRx predicted that
466 mifepristone inhibits cardiomyocyte hypertrophy through a glucocorticoid receptor - LCK – ERK
467 pathway, which we validated in two contexts in cultured cardiomyocytes. The implications of
468 mifepristone for repurposing against cardiac hypertrophy warrant further investigation.

469 Machine learning methods that not only predict efficacy but also pathway mechanisms are
470 greatly needed. Here, we developed a mechanistic machine learning method LogiRx to discover
471 pathways by which escitalopram and mifepristone inhibit cardiomyocyte hypertrophy. These pathways

472 were validated in cultured cells in two contexts. Escitalopram decreased cardiomyocyte hypertrophy in
473 vivo and was associated with a lower incidence of cardiac hypertrophy in two patient cohorts. Together,
474 these studies demonstrate the ability of LogiRx to predict drug efficacy and mechanisms that guide new
475 experiments.
476

477 **Acknowledgments**

478 We thank Mohammad Fallahi-Sichani for use of his Perkin Elmer Operetta, statistical consulting from
479 Marieke Jones, manuscript feedback from Kevin Janes and Jason Papin, and Malcolm O'Malley for
480 naming LogiRx.
481

482 **References**

483 1. Frey, N., Katus, H. A., Olson, E. N. & Hill, J. A. Hypertrophy of the Heart. *Circulation* **109**, 1580–1589
484 (2004).
485 2. Samak, M. *et al.* Cardiac Hypertrophy: An Introduction to Molecular and Cellular Basis. *Med. Sci.*
486 *Monit. Basic Res.* **22**, 75–79 (2016).
487 3. Nomura, S. *et al.* Cardiomyocyte gene programs encoding morphological and functional signatures in
488 cardiac hypertrophy and failure. *Nat. Commun.* **9**, 4435 (2018).
489 4. Marian, A. J. 23 - Heart Failure as a Consequence of Hypertrophic Cardiomyopathy. in *Heart Failure: a*
490 *Companion to Braunwald's Heart Disease (Fourth Edition)* (eds. Felker, G. M. & Mann, D. L.) 311-
491 321.e6 (Elsevier, Philadelphia, 2020). doi:10.1016/B978-0-323-60987-6.00023-5.
492 5. Bazgir, F. *et al.* The Microenvironment of the Pathogenesis of Cardiac Hypertrophy. *Cells* **12**, 1780
493 (2023).
494 6. Xie, M., Burchfield, J. S. & Hill, J. A. Pathological Ventricular Remodeling: Mechanisms: Part 1 of 2.
495 *Circulation* **128**, 388–400 (2013).

496 7. Tham, Y. K., Bernardo, B. C., Ooi, J. Y. Y., Weeks, K. L. & McMullen, J. R. Pathophysiology of cardiac
497 hypertrophy and heart failure: signaling pathways and novel therapeutic targets. *Arch. Toxicol.* **89**,
498 1401–1438 (2015).
499 8. Tsao, C. W. *et al.* Heart Disease and Stroke Statistics-2023 Update: A Report From the American Heart
500 Association. *Circulation* **147**, e93–e621 (2023).
501 9. Schubert, M., Hansen, S., Leefmann, J. & Guan, K. Repurposing Antidiabetic Drugs for Cardiovascular
502 Disease. *Front. Physiol.* **11**, 568632 (2020).
503 10. Onódi, Z., Koch, S., Rubinstein, J., Ferdinandy, P. & Varga, Z. V. Drug repurposing for
504 cardiovascular diseases: New targets and indications for probenecid. *Br. J. Pharmacol.* **180**, 685–700
505 (2023).
506 11. Xie, Y. *et al.* Mechanisms of SGLT2 Inhibitors in Heart Failure and Their Clinical Value. *J.*
507 *Cardiovasc. Pharmacol.* **81**, 4–14 (2023).
508 12. Reid, B. G. *et al.* Discovery of novel small molecule inhibitors of cardiac hypertrophy using high
509 throughput, high content imaging. *J. Mol. Cell. Cardiol.* **97**, 106–113 (2016).
510 13. Dukinfield, M. *et al.* Repurposing an anti-cancer agent for the treatment of hypertrophic heart
511 disease. *J. Pathol.* **249**, 523–535 (2019).
512 14. Escudero, D. S. *et al.* PDE5 inhibition improves cardiac morphology and function in SHR by
513 reducing NHE1 activity: Repurposing Sildenafil for the treatment of hypertensive cardiac hypertrophy.
514 *Eur. J. Pharmacol.* **891**, 173724 (2021).
515 15. Wang, Z. *et al.* A high-throughput drug screening identifies luteolin as a therapeutic candidate
516 for pathological cardiac hypertrophy and heart failure. *Front. Cardiovasc. Med.* **10**, 1130635 (2023).
517 16. Nakamura, M. & Sadoshima, J. Mechanisms of physiological and pathological cardiac
518 hypertrophy. *Nat. Rev. Cardiol.* **15**, 387–407 (2018).

519 17. Sun, J., Yang, J., Chi, J., Ding, X. & Lv, N. Identification of drug repurposing candidates based on a
520 miRNA-mediated drug and pathway network for cardiac hypertrophy and acute myocardial
521 infarction. *Hum. Genomics* **12**, 52 (2018).
522 18. Rai, A., Kumar, V., Jerath, G., Kartha, C. C. & Ramakrishnan, V. Mapping drug-target interactions
523 and synergy in multi-molecular therapeutics for pressure-overload cardiac hypertrophy. *NPJ Syst.*
524 *Biol. Appl.* **7**, 11 (2021).
525 19. Ryall, K. *et al.* Network reconstruction and systems analysis of cardiac myocyte hypertrophy
526 signaling. *J. Biol. Chem.* **287**, 42259–42268 (2012).
527 20. Khalilimeybodi, A., Paap, A. M., Christiansen, S. L. M. & Saucerman, J. J. Context-specific network
528 modeling identifies new crosstalk in β-adrenergic cardiac hypertrophy. *PLoS Comput. Biol.* **16**, (2020).
529 21. Wishart, D. S. *et al.* DrugBank 5.0: a major update to the DrugBank database for 2018. *Nucleic*
530 *Acids Res.* **46**, D1074–D1082 (2018).
531 22. Türei, D., Korcsmáros, T. & Saez-Rodriguez, J. OmniPath: guidelines and gateway for literature-
532 curated signaling pathway resources. *Nat. Methods* **13**, 966–967 (2016).
533 23. Ceccarelli, F., Turei, D., Gabor, A. & Saez-Rodriguez, J. Bringing data from curated pathway
534 resources to Cytoscape with OmniPath. *Bioinformatics* **36**, 2632–2633 (2020).
535 24. Gil, D. P., Law, J. N. & Murali, T. M. The PathLinker app: Connect the dots in protein interaction
536 networks. *F1000Research* **6**, 58 (2017).
537 25. Ritz, A. *et al.* Pathways on demand: automated reconstruction of human signaling networks. *NPJ*
538 *Syst. Biol. Appl.* **2**, 16002 (2016).
539 26. Shannon, P. *et al.* Cytoscape: A Software Environment for Integrated Models of Biomolecular
540 Interaction Networks. *Genome Res.* **13**, 2498–2504 (2003).
541 27. Zeigler, A. C. *et al.* Network model-based screen for FDA-approved drugs affecting cardiac
542 fibrosis. *CPT Pharmacomet. Syst. Pharmacol.* **10**, 377–388 (2021).

543 28. Eggertsen, T. G. & Saucerman, J. J. Virtual drug screen reveals context-dependent inhibition of
544 cardiomyocyte hypertrophy. *Br. J. Pharmacol.* **180**, 2721–2735 (2023).
545 29. Van de Graaf, M. W., Eggertsen, T. G., Zeigler, A. C., Tan, P. M. & Saucerman, J. J. Benchmarking
546 of protein interaction databases for integration with manually reconstructed signalling network
547 models. *J. Physiol.* (2023) doi:10.1113/JP284616.
548 30. Stirling, D. R. *et al.* CellProfiler 4: improvements in speed, utility and usability. *BMC*
549 *Bioinformatics* **22**, 433 (2021).
550 31. Bass, G. T. *et al.* Automated image analysis identifies signaling pathways regulating distinct
551 signatures of cardiac myocyte hypertrophy. *J. Mol. Cell. Cardiol.* **52**, 923–930 (2012).
552 32. Sarangdhar, M. *et al.* Data mining differential clinical outcomes associated with drug regimens
553 using adverse event reporting data. *Nat. Biotechnol.* **34**, 697–700 (2016).
554 33. Yap, T. A. *et al.* First-in-Human Phase I Trial of Two Schedules of OSI-930, a Novel Multikinase
555 Inhibitor, Incorporating Translational Proof-of-Mechanism Studies. *Clin. Cancer Res. Off. J. Am. Assoc.*
556 *Cancer Res.* **19**, 10.1158/1078-0432.CCR-12–2258 (2013).
557 34. Chan, S. H. Y., Khatib, Y., Webley, S., Layton, D. & Salek, S. Identification of cardiotoxicity related
558 to non-small cell lung cancer (NSCLC) treatments: A systematic review. *Front. Pharmacol.* **14**,
559 1137983 (2023).
560 35. Xu, Z. *et al.* Inhibition of PRKAA/AMPK (Ser485/491) phosphorylation by crizotinib induces
561 cardiotoxicity via perturbing autophagosome-lysosome fusion. *Autophagy* **20**, 416–436.
562 36. Kasper, S. *et al.* Differences in the dynamics of serotonin reuptake transporter occupancy may
563 explain superior clinical efficacy of escitalopram versus citalopram. *Int. Clin. Psychopharmacol.* **24**,
564 119–125 (2009).
565 37. Sanchez, C., Reines, E. H. & Montgomery, S. A. A comparative review of escitalopram,
566 paroxetine, and sertraline: are they all alike? *Int. Clin. Psychopharmacol.* **29**, 185 (2014).

567 38. Kasner, M. T. *et al.* A phase Ib dose escalation study of oral monotherapy with KX2-391 in elderly
568 patients with acute myeloid leukemia. *Invest. New Drugs* **40**, 773–781 (2022).
569 39. Crabol, Y., Catherinot, E., Veziris, N., Jullien, V. & Lortholary, O. Rifabutin: where do we stand in
570 2016? *J. Antimicrob. Chemother.* **71**, 1759–1771 (2016).
571 40. Pivonello, R., De Leo, M., Cozzolino, A. & Colao, A. The Treatment of Cushing's Disease. *Endocr.*
572 *Rev.* **36**, 385–486 (2015).
573 41. Hajialyani, M. *et al.* Hesperidin as a Neuroprotective Agent: A Review of Animal and Clinical
574 Evidence. *Mol. Basel Switz.* **24**, 648 (2019).
575 42. Thase, M. E., Larsen, K. G., Reines, E. & Kennedy, S. H. The cardiovascular safety profile of
576 escitalopram. *Eur. Neuropsychopharmacol. J. Eur. Coll. Neuropsychopharmacol.* **23**, 1391–1400
577 (2013).
578 43. Kimura, K. *et al.* Cardiovascular adverse reactions associated with escitalopram in patients with
579 underlying cardiovascular diseases: a systematic review and meta-analysis. *Front. Psychiatry* **14**,
580 1248397 (2023).
581 44. Heppt, M. V. *et al.* Comparative Efficacy and Safety of Tirbanibulin for Actinic Keratosis of the
582 Face and Scalp in Europe: A Systematic Review and Network Meta-Analysis of Randomized Controlled
583 Trials. *J. Clin. Med.* **11**, 1654 (2022).
584 45. Darpo, B., Bullingham, R., Combs, D. L., Ferber, G. & Hafez, K. Assessment of the cardiac safety
585 and pharmacokinetics of a short course, twice daily dose of orally-administered mifepristone in
586 healthy male subjects. *Cardiol. J.* **20**, 152–160 (2013).
587 46. Mathew, S., Ticsa, M. S., Qadir, S., Rezene, A. & Khanna, D. Multiple Clinical Indications of
588 Mifepristone: A Systematic Review. *Cureus* **15**, e48372.

589 47. Phillips, M. C., Wald-Dickler, N., Loomis, K., Luna, B. M. & Spellberg, B. Pharmacology, Dosing,
590 and Side Effects of Rifabutin as a Possible Therapy for Antibiotic-Resistant Acinetobacter Infections.
591 *Open Forum Infect. Dis.* **7**, ofaa460 (2020).
592 48. Ikeda, K. *et al.* The effects of sarpogrelate on cardiomyocyte hypertrophy. *Life Sci.* **67**, 2991–
593 2996 (2000).
594 49. Shimizu, K. *et al.* The Selective Serotonin 2A Receptor Antagonist Sarpogrelate Prevents Cardiac
595 Hypertrophy and Systolic Dysfunction via Inhibition of the ERK1/2–GATA4 Signaling Pathway.
596 *Pharmaceuticals* **14**, 1268 (2021).
597 50. Vadas, O. *et al.* Molecular determinants of PI3Kγ-mediated activation downstream of G-protein–
598 coupled receptors (GPCRs). *Proc. Natl. Acad. Sci.* **110**, 18862–18867 (2013).
599 51. Aghajanian, H. *et al.* Targeting Cardiac Fibrosis with Engineered T cells. *Nature* **573**, 430–433
600 (2019).
601 52. Palandri, C. *et al.* Pharmacological Management of Hypertrophic Cardiomyopathy: From Bench
602 to Bedside. *Drugs* **82**, 889–912 (2022).
603 53. Sapna, F. *et al.* Advancements in Heart Failure Management: A Comprehensive Narrative Review
604 of Emerging Therapies. *Cureus* **15**, e46486.
605 54. Abdelsayed, M., Kort, E. J., Jovinge, S. & Mercola, M. Repurposing drugs to treat cardiovascular
606 disease in the era of precision medicine. *Nat. Rev. Cardiol.* **19**, 751–764 (2022).
607 55. Kirouac, D. *et al.* Creating and analyzing pathway and protein interaction compendia for
608 modelling signal transduction networks. *BMC Syst. Biol.* **6**, 29 (2012).
609 56. Chen, B., Fan, W., Liu, J. & Wu, F.-X. Identifying protein complexes and functional modules--from
610 static PPI networks to dynamic PPI networks. *Brief. Bioinform.* **15**, 177–194 (2014).
611 57. Kabir, M. H., Patrick, R., Ho, J. W. K. & O'Connor, M. D. Identification of active signaling
612 pathways by integrating gene expression and protein interaction data. *BMC Syst. Biol.* **12**, 120 (2018).

613 58. Liu, A. *et al.* From expression footprints to causal pathways: contextualizing large signaling
614 networks with CARNIVAL. *NPJ Syst. Biol. Appl.* **5**, 40 (2019).
615 59. Frank, D. U., Sutcliffe, M. D. & Saucerman, J. J. Network-based predictions of in vivo cardiac
616 hypertrophy. *J. Mol. Cell. Cardiol.* **121**, 180–189 (2018).
617 60. Zeigler, A. C., Richardson, W. J., Holmes, J. W. & Saucerman, J. J. A computational model of
618 cardiac fibroblast signaling predicts context-dependent drivers of myofibroblast differentiation. *J.*
619 *Mol. Cell. Cardiol.* **94**, 72–81 (2016).
620 61. Nelson, A. R., Christiansen, S. L., Naegle, K. M. & Saucerman, J. J. Logic-based mechanistic
621 machine learning on high-content images reveals how drugs differentially regulate cardiac
622 fibroblasts. *Proc. Natl. Acad. Sci. U. S. A.* **121**, e2303513121 (2024).
623 62. Bouhaddou, M. *et al.* A mechanistic pan-cancer pathway model informed by multi-omics data
624 interprets stochastic cell fate responses to drugs and mitogens. *PLoS Comput. Biol.* **14**, e1005985
625 (2018).
626 63. Keenan, A. B. *et al.* The Library of Integrated Network-Based Cellular Signatures NIH Program:
627 System-Level Cataloging of Human Cells Response to Perturbations. *Cell Syst.* **6**, 13–24 (2018).
628 64. Ahmed, L. A., Shiha, N. A. & Attia, A. S. Escitalopram Ameliorates Cardiomyopathy in Type 2
629 Diabetic Rats via Modulation of Receptor for Advanced Glycation End Products and Its Downstream
630 Signaling Cascades. *Front. Pharmacol.* **11**, 579206 (2020).
631 65. Bush, E. *et al.* A small molecular activator of cardiac hypertrophy uncovered in a chemical screen
632 for modifiers of the calcineurin signaling pathway. *Proc. Natl. Acad. Sci. U. S. A.* **101**, 2870–2875
633 (2004).
634 66. Mialet-Perez, J. *et al.* Serotonin 5-HT2A receptor-mediated hypertrophy is negatively regulated
635 by caveolin-3 in cardiomyoblasts and neonatal cardiomyocytes. *J. Mol. Cell. Cardiol.* **52**, 502–510
636 (2012).

637 67. Gao, W. *et al.* HTR2A promotes the development of cardiac hypertrophy by activating PI3K-
638 PDK1-AKT-mTOR signaling. *Cell Stress Chaperones* **25**, 899–908 (2020).
639 68. Schumacher, S. M. *et al.* Paroxetine-mediated GRK2 inhibition reverses cardiac dysfunction and
640 remodeling after myocardial infarction. *Sci. Transl. Med.* **7**, 277ra31 (2015).
641 69. Thal, D. M. *et al.* Paroxetine is a direct inhibitor of g protein-coupled receptor kinase 2 and
642 increases myocardial contractility. *ACS Chem. Biol.* **7**, 1830–1839 (2012).
643 70. Sun, X. *et al.* Paroxetine Attenuates Cardiac Hypertrophy Via Blocking GRK2 and ADRB1
644 Interaction in Hypertension. *J. Am. Heart Assoc. Cardiovasc. Cerebrovasc. Dis.* **10**, e016364 (2020).
645 71. Bouley, R. *et al.* Structural Determinants Influencing the Potency and Selectivity of Indazole-
646 Paroxetine Hybrid G Protein-Coupled Receptor Kinase 2 Inhibitors. *Mol. Pharmacol.* **92**, 707–717
647 (2017).
648 72. Ferrero, K. M. & Koch, W. J. GRK2 in cardiovascular disease and its potential as a therapeutic
649 target. *J. Mol. Cell. Cardiol.* **172**, 14–23 (2022).
650 73. Ren, R., Oakley, R. H., Cruz-Topete, D. & Cidlowski, J. A. Dual Role for Glucocorticoids in
651 Cardiomyocyte Hypertrophy and Apoptosis. *Endocrinology* **153**, 5346–5360 (2012).
652 74. Severinova, E. *et al.* Glucocorticoid Receptor-Binding and Transcriptome Signature in
653 Cardiomyocytes. *J. Am. Heart Assoc.* **8**, e011484 (2019).
654 75. Oakley, R. H. *et al.* Essential role of stress hormone signaling in cardiomyocytes for the
655 prevention of heart disease. *Proc. Natl. Acad. Sci. U. S. A.* **110**, 17035–17040 (2013).
656 76. Pianca, N. *et al.* Glucocorticoid receptor antagonization propels endogenous cardiomyocyte
657 proliferation and cardiac regeneration. *Nat. Cardiovasc. Res.* **1**, 617–633 (2022).
658
659